# Chapter 8

# PEG-induced morphologically unstable growth of tetragonal hen egg-white lysozyme crystals

Poly(ethylene glycol) (PEG) is an often used crystallising agent in screening experiments for protein crystallisation conditions. To investigate the influence of poly(ethylene glycol)-4600 on the diffusion process during protein crystal growth, a series of in-situ optical microscopy experiments was performed in which the diffusion coefficient was changed by the addition of PEG. Depending on the balance between diffusion coefficient and driving force, lysozyme crystals were found to grow faceted, kinetically rough, or morphologically unstable. In-situ observations show the development of a lysozyme crystal from polyhedral stability to instability and back to stability again as the balance changes within one experiment. A stability diagram showing the occurrence of morphological instability based on the starting conditions is presented, showing that kinetic roughening stabilises the crystal morphology. The results are interpreted in terms of a competition between 2D nucleation at the edges of the crystal and step flow on its surface. In this, surface protein concentration

profiles derived from observed crystal shapes are used.

## 8.1 Introduction

X-ray diffraction (XRD) is the main route towards structure determination of protein macromolecules. The success of structure determination by this method depends on the quality of the protein crystal, which is typically grown from an aqueous solution. In screening experiments for successful crystallisation conditions, poly(ethylene-glycol) (PEG) is often used as a precipitating agent additional to salts[1–4]. The addition of PEG reduces the solubility of proteins by steric exclusion[5] and thus stimulates nucleation and growth. The effectiveness of the added PEG depends on the concentration and its molecular weight[6, 7].

Besides acting as a precipitating agent, PEG also lowers the diffusion coefficient for proteins in the solution[8]. The rate of diffusion is relevant in crystal growth systems in which natural convection is reduced, for instance experiments in microgravity[9], using nanoliter volumes[10, 11], using gels[12–14], and damping of convection by magnetic fields[15]. Such systems are of interest because convection is thought to have a negative influence on crystal quality as it is an effective means for impurities to be transported towards the crystal surface[16].

Mass transport towards the crystal surface and surface kinetics (i.e. surface diffusion and incorporation of growth units) together determine the growth rate of the crystal. In convective systems mass transport is generally faster than surface kinetics, and surface kinetics is the rate limiting step. In systems where diffusion, which is typically two orders of magnitude slower than convection[17], is the sole means of mass transport, this balance is shifted towards equal contributions or even towards mass transport limitation. As a result, local differences in surface concentration are not compensated anymore by surface kinetics and the crystal looses its faceted form and becomes hopper shaped or grows in a dendritic fashion; in other words, the crystal looses its morphological stability[18, 19]. The occurrence of such instabilities not only

depends on the balance between diffusion and surface kinetics, but also on crystal size and supersaturation[20]. In protein crystal growth, surface kinetics are generally very slow[21, 22] and, for instance, lysozyme crystals grown under typical circumstances are expected to be stable up to 2-4 cm in size[23], which is very large for protein crystals. The occurrence of morphological instability is relevant to protein crystal growth as it can cause striations and lattice defects which are detrimental to crystal quality[24–26].

In this paper, we present a study on the influence of PEG-4600 on the macroscopic morphological stability of tetragonal hen egg-white lysozyme crystals grown in thin cells ($\sim$100 $\mu$m), mimicking the nowadays often used crystallisation technique of nanoliter volumes[3, 10, 11] in combination with the use of precipitation enhancers. The growth kinetics of morphologically unstable HEWL crystals are studied by in-situ optical microscopy in a systematic screening of growth morphology for various combinations of PEG-4600 concentration, lysozyme concentration and temperature. We present a "stability diagram" in which the transition from faceted to unstable tetragonal lysozyme crystals, induced by the addition of PEG, is expressed in terms of supersaturation and the diffusion coefficient. The results are interpreted in terms of a competition between 2D nucleation at the edges of the crystal and step flow on its surface.

## 8.2 Experimental procedures

Chemicals of analytical grade were used in this study. A buffer stock solution of sodium acetate and acetic acid was made in deionised water (>15 M$\Omega$cm) to result in a 0.05 M NaOAc/HOAc solution of pH 4.5. HEWL from Sigma-Aldrich (lot nr. 094K1454) in buffer was used as source material for crystal growth after reducing the lower MW contaminants by dialysis (MWCO 8 kDa) against the buffer solution. MALDI-TOF measurements did not reveal contaminations of higher MW. NaCl stock solutions of 1.37 M were prepared in buffer solution, filtered over a 0.2 $\mu$m membrane (Schleicher & Schuell) and mixed with PEG-4600 (Sigma-Aldrich) to obtain twice the PEG

and NaCl concentration required in experiment. Lysozyme stock solutions and buffer solutions were filtered over a 0.2 membrane and mixed to obtain a solution containing twice the required HEWL concentration for the experiment. HEWL-buffer and NaCl-PEG-buffer solutions were mixed one-to-one prior to experiments. Thus, all experiments were performed in a 0.685 M NaCl (4%w/v) and 0.05 M NaOAc/HOAc solution of pH 4.5. We determined the pH to vary linearly with PEG concentration following pH=4.50+0.01·[PEG], with [PEG] in %w/v.

A 10 $\mu$l droplet of the resulting mother liquor is placed on a sapphire window and a cover-slide is placed on top. The droplet forms an approximately 100 $\mu$m thick layer and is sealed off at the sides by vacuum grease to prevent evaporation of the solution. The small spacing in the vertical direction prevents the formation of free convection patterns, and mass transport during crystal growth is only determined by diffusion[26]. The sapphire window is placed in a temperature controlled cell for in-situ microscopy. Using sapphire instead of regular glass ensures a better heat conductivity and thus better temperature control of the system. Experiments were performed at temperatures between 9 $^o$C and 20 $^o$C with an accuracy of 0.1 $^o$C. The in-situ cell consists of a brass plate through which water from a thermostatically controlled reservoir can flow. The sample is placed on top of the brass plate and covered by another brass plate without water through-put. Holes in the middle of the two brass plates allow for optical transmission microscopy.

Series of time-lapse micrographs were made using an Olympus Vanox optical microscope in combination with a Nikon DS5M CCD camera. Image processing software (ImagePro Plus[27]) and Matlab[28] were used to automatically acquire the crystal size and shape from subsequent images of the time-lapse series.

## 8.3 Results and Discussion

### 8.3.1 Morphological instability

In figure 8.1 a series of photographs shows a typical morphologically unstable growth experiment, performed at 10.5 $^o$C with 30 mg/ml HEWL and 10% w/v PEG-4600. The images show a tetragonal lysozyme crystal viewed along its *c*-axis, which is also the four-fold symmetry axis of its $P4_32_12$ crystal structure; the sides are the {110} faces. In the first image of the experiment, about 4 minutes after placing the sample in the temperature controlled cell, the crystal is approximately 20 by 20 $\mu$m and nicely faceted. After just a few minutes, when the crystal is approximately 30 by 30 $\mu$m in size, it starts to loose its morphological stability. The crystal grows faster at the corners than in middle of the {110} side faces, which become concave and have re-entrant corners appearing in the middle.

The development of morphological instability is a result of an inhomogeneous concentration distribution at the crystal surface. For a square crystal growing from solution (figure 8.2a), experiment[29], conformal transformation [30] and numerical simulations [20] show that the concentration profile is approximately circular, and intersects the crystal surface. As the growth rate of a crystal depends on the surface concentration, the corners grow faster than the middle of the crystal faces (figure 8.2b). Thus, the morphological instability is the result of a square crystal being present in an approximately circular concentration field. Therefore, this kind of instability is also called polyhedral instability and is different from the instability due to perturbations as described by Mullins and Sekerka[31, 32].

Polyhedral instability can be regarded as the result of the competition between 2D nucleation of islands near the edges and corners of the surface and the subsequent spread of these islands over the crystal surface. For a small crystal the supersaturation difference between edge and middle of the surface is small, and 2D nucleation, exponentially dependent on the supersaturation, is much slower than step flow over the surface, which changes approximately linearly with supersaturation. While the crystal grows, the supersaturation

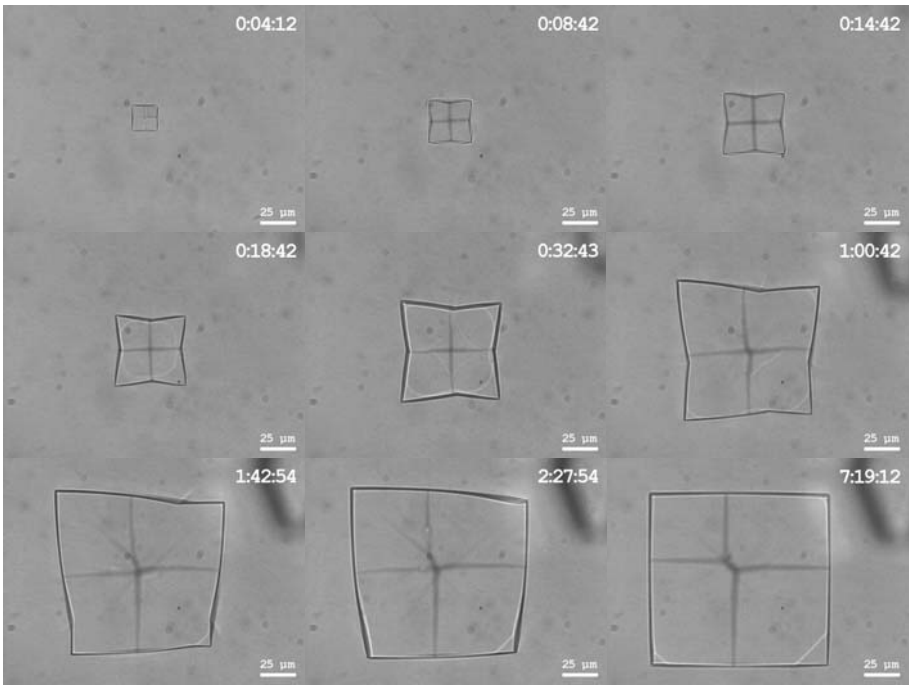


**Figure 8.1:** Series of images of a tetragonal hen egg-white lysozyme crystal which becomes morphologically unstable, but in the end regains its stability due to the exhaustion of the mother liquor. The time in the upper right corner of the images indicates hours, minutes and seconds since the sample was placed in the temperature controlled cell at 10.5 $^o$C. The initial mother liquor consists of 30 mg/ml HEWL, 0.685 M NaCl, 10 % w/v PEG-4600 and 0.05 M NaOAc/HOAc buffer of pH 4.5. The scalebars indicate 25 $\mu$m.

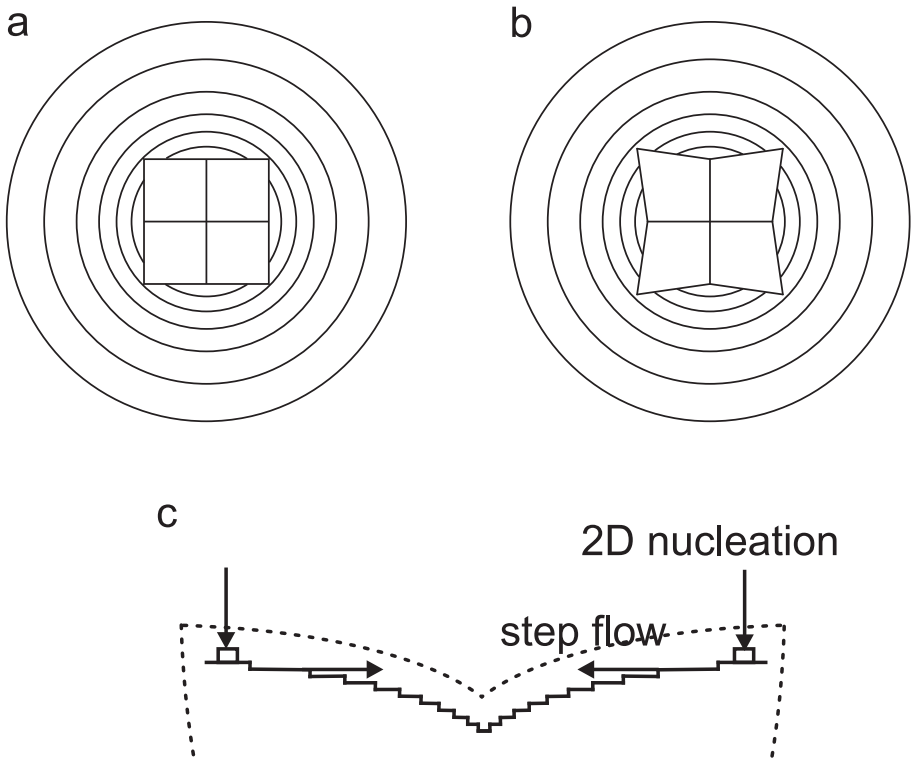


**Figure 8.2:** a) Schematic representation of the concentration profile around a growing tetragonal lysozyme crystal, viewed along its *c*-axis. The iso-concentration lines intersect the crystal surface. b) As a result, the edges and corners grow faster than the middle of the crystal faces. c) Principle of the morphologically unstable growth, resulting from the competition of 2D nucleation at the corners and edges due to the locally high supersaturation and subsequent step flow toward the middle. The dashed line indicates the macroscopic continuous crystal shape made up of microscopic, discrete steps.

difference between edge and middle becomes larger until at some point at the edges and corners new islands are formed faster than the previous ones completely cover the surface (figure 8.2c). As a result, the corners and edges of the crystal grow faster than the face centres and the crystal morphology becomes unstable.

Due to the finite supply of lysozyme molecules in the closed system, in the long run the overall solute content and thus the surface concentration drops. The supersaturation decreases and the crystal regains its morphological stability (figure 8.1) because the step flow is now faster again than 2D nucleation. This leads to a square, faceted crystal shape at the end of the experiment. In this later stage of growth, the crystal as a whole first develops in a slightly asymmetric fashion due to the presence of other crystals in its surroundings. This asymmetry, like the instability, is corrected when the surface supersaturation drops. However, the temporary asymmetry in the supply of lysozyme molecules to the crystal remains visible in the size difference of the {101} faces, as can often be encountered in lysozyme crystal growth experiments at higher supersaturation.

### 8.3.2 Stability diagram

To investigate the conditions at which growing tetragonal lysozyme crystals experience morphological instability, temperature, PEG-4600 concentration and lysozyme concentration were varied. Crystals were observed during growth by optical microscopy to check if they develop any instability. As the instability of a crystal partly depends on its size, a crystal might become unstable at larger sizes than observed during experiment. However, depending on starting conditions, on average a certain number of crystals will nucleate per unit volume, and deplete the solution while growing. Thus, depending on the starting conditions, the crystals have a certain maximum size depending on the available material. We call a condition “stable” if during the experiment, i.e. from nucleation to growth cessation, crystals do not show instability. The initial conditions for which morphologically unstable growth occurs are shown in the ”stability diagram” of figure 8.3a.

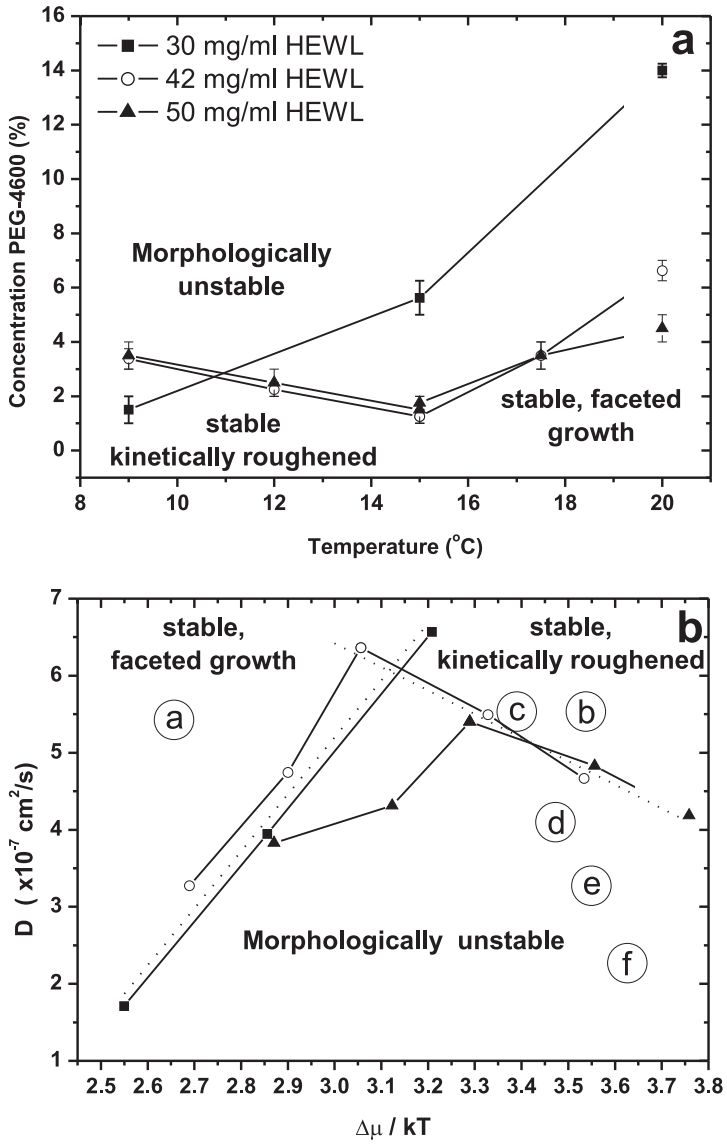


**Figure 8.3:** a) Instability diagram for the HEWL/NaCl/PEG-4600 system, with 0.685 M NaCl and 0.05 M NaOAc buffer solution at pH 4.5. b) Same data as in panel a, but now in terms of diffusion coefficient and driving force. The letters correspond to the panels of figure 8.4 showing crystals grown at these conditions.

In the stable region, lysozyme crystals develop as polyhedral crystals, with well-defined {110} and {101} faces (figure 8.4a). Increasing temperature, PEG-4600 concentration, lysozyme concentration or any combination of these parameters, brings the system into the unstable region. While in the unstable zone, the extent of instability depends on the conditions' distance to the stable zone. Figures 8.4d up to f show unstable lysozyme crystals at increasingly destabilising conditions. Figure 8.4f is close to growth in a dendritic fashion, as the reentrant corners suffer from a severe lack of growth units.

A third region at higher supersaturation is present in which the crystals are neither faceted nor unstable, but kinetically rough[33] (see figures 8.4b and c). Kinetically rough growth is a result of a high driving force, which reduces the critical nucleus size for 2D nucleation to equal or below the size of one growth unit[34]. As a result, the anisotropy in growth rates normally resulting in the formation of facets disappears and the surfaces get rounded and convex. Due to the rounded shape -which in some cases is even almost cylindrical, as shown in figure 8.4b*- polyhedral instability is reduced.

Although for practical purposes figure 8.3 suffices, for comparison of mass transport and surface kinetics conditions, one would like to have the stability as function of diffusion coefficient, driving force and crystal size instead of PEG concentration and temperature. In our experiments we usually find that instability starts to develop when the crystals have a size of 20 to 30 $\mu$m. The driving force for crystallisation is given by

$$\frac{\Delta\mu}{kT} = \ln\frac{c}{c_{\mathrm{eq}}} \ , \tag{8.1}$$

in which $c$ is the lysozyme concentration, and $c_{\mathrm{eq}}$ the equilibrium lysozyme concentration under given conditions. To convert lysozyme concentration to driving force, we use literature data on the equilibrium concentration at various temperatures for lysozyme in solutions as used in our experiments[35]. These data do not include added polyethylene-glycols. The equilibrium concentration

*The {101} faces have different step energy and thus kinetic roughening sets on at a higher driving force.

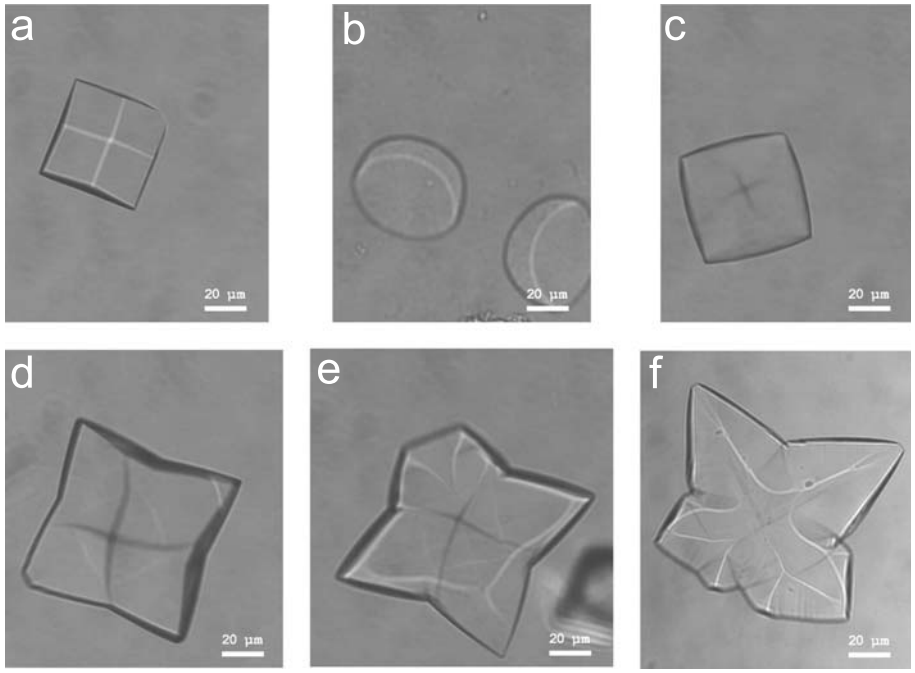


**Figure 8.4:** Examples of tetragonal lysozyme crystals grown under different conditions, all from a 0.685 M NaCl/0.05 M NaOAc buffer solution of pH 4.5. The scalebars indicate 20 $\mu$m. a) stable growth at 50 mg/ml HEWL, 0 %w/v PEG-4600 and 20 $^o$C. For panels b up to e conditions are identical, 50 mg/ml and 9 $^o$C, except for an increase in PEG-4600 concentration. b) kinetically rough growth at 0 %w/v PEG-4600. c) kinetically rough growth at 2 %w/v PEG-4600. d) morphologically unstable growth at 5 %w/v PEG-4600. e) morphologically unstable growth at 10 %w/v PEG-4600. f) morphologically unstable growth at 40 mg/ml HEWL, 25 %w/v PEG-4600 and 20 $^o$C.

varies with PEG-concentration as well, and its dependence is given by[6]

$$\ln c_{\mathrm{eq}} = \ln c_{\mathrm{eq},0} - K[\mathrm{PEG}] \ , \tag{8.2}$$

in which $c_{\mathrm{eq},0}$ is the equilibrium concentration without PEG added, [PEG] the polyethylene-glycol concentration in % w/v, and $K$ a proportionality constant. We determined $K$ by solubility experiments to be approximately 0.02.

The diffusion coefficient of lysozyme changes with the addition of polyethylene-glycols[8], but also decreases with increasing lysozyme concentration[36]. The dependency of the diffusion coefficient on lysozyme concentration is given by[36]

$$D = D_0 \left[1 + k_D \phi\right] \ , \tag{8.3}$$

where $\phi$ is the volume fraction of lysozyme, $k_D$ the diffusivity slope, and $D_0$ the single particle diffusion coefficient. The diffusivity slope depends on the exact solvent composition, i.e. both sodium acetate concentration and sodium chloride concentration. In our calculations we use the value -12.1 for 0.427 M NaCl as an upper limit as the slope $k_D$ is expected to be slightly steeper for 0.685 M. Thus, the diffusion constant for higher lysozyme concentration is slightly overestimated, and mass transport is even slower. To include the effect of PEG-4600 on the diffusion constant, we use data on the reduced viscosity of PEG-4000 in water[5]. The effect of PEG on diffusion is mainly an effect of increase in viscosity[8]. The single particle diffusion $D_0$ is related to the dynamic viscosity through the Stokes-Einstein relation

$$D_0 = \frac{k_B T}{6\pi\eta a_H} \ , \tag{8.4}$$

where $\eta$ is the dynamic viscosity of the solvent, and $a_h$ $\sim$1.7 nm the hydrodynamic radius of a lysozyme molecule[37]. As an approximation we consider the added PEG-4600 to change the viscosity in equation 8.4, and thus also $D_0$ in equation 8.3. In this way, the diffusion coefficient is calculated using lysozyme concentration and PEG-4600 concentration. The appropriate driving forces and diffusion coefficients determined in this way are used in the stability diagram of figure 8.3b.

The stability diagram of figure 8.3b suggests that a simple, empirical criterion based on diffusion coefficient and driving force should be indicative of the polyhedral stability of tetragonal lysozyme crystals. The diffusion coefficient indicates the speed of the mass transport process, while the initial supersaturation determines the maximum growth rate of the crystal. From experiments, we find a stability criterion

$$\xi = \frac{-17 + 7.4 \times \Delta\mu/kT}{D \times 10^7} \ , \tag{8.5}$$

where $D$ is the diffusion coefficient in $\mathrm{cm}^2/\mathrm{s}$. For $\xi < 1$, crystals can be expected to retain their stability, while for $\xi > 1$ the balance between surface kinetics and transport will induce morphological instability. It should be realised that the above mentioned stability criterion only holds for the present growth system. Changing the type of salt may result in different polymorphs, which have different energetics, and even changing salt concentration may change the polymorph[38] and growth mode[33].

The stability criterion for kinetically roughened crystals is very different from the faceted ones, being

$$\zeta = \frac{16 - 3.1 \times \Delta\mu/kT}{D \times 10^7} \ . \tag{8.6}$$

Here, the factor before $\Delta\mu/kT$ is now *negative*, i.e. morphological stability increases for increasing supersaturation. This effect, which is surprising, can be understood in terms of the polyhedral nature of the instabilities. Slightly rounded crystals will experience a lower supersaturation difference than properly faceted crystals, because the surface more closely follows the cylindrical concentration profile. For a rounded, cornerless crystal obtained at the highest $\Delta\mu/kT$, no supersaturation difference between corner and middle can even exist.

### 8.3.3 Dynamic aspects

As is clear from the series of images of figure 8.1, morphological instability is a transient state. Series of images like those of figure 8.1 offer the possibility to acquire quantitative data on growth rates and stability of lysozyme

crystals. Figure 8.5a shows the corner-to-corner distance and the middle-to-middle distance of the crystal in figure 8.1. These are determined by using the software program ImagePro Plus to automatically acquire the maximum and minimum diameter of the crystals in the optical images, as indicated by the red and black arrows respectively in figure 8.6. From the maximum diameter the corner-to-corner distance is derived by using Pythagoras' theorem (blue arrows in figure 8.6). The solid line in figure 8.5a indicates the ratio between middle-to-middle and corner-to-corner distance. This ratio in combination with its time-derivative is a benchmark for the stability of the crystal. A ratio of one indicates a square crystal (figure 8.6a). If the ratio is smaller than one (figure 8.6b) and decreasing, the crystal is morphologically unstable. If the ratio is smaller than one but the ratio increases, the crystal is stable and recovering its square form. Using the method of the minimum and maximum diameter has the extra benefit that kinetic roughness can also be adjudicated by this ratio, as for circular crystal shapes and square crystals with rounded corners it is larger than one (figure 8.6c).

In the example of the experiment of figure 8.1, the stability of the crystal decreases up to 55 minutes after the start of the experiment. At this point, the growth rates of the face centres become larger than those of the corners (figure 8.5b), and the stability ratio increases as the crystal regains its stability. Theoretically, the instability should increase while the crystal continues to grow. However, the growing crystal and also other crystals nucleated in the solution deplete their surroundings from lysozyme molecules. When the diffusion field of a crystal starts to overlap with that of neighbouring crystals, the growth rate drops. This moment coincides with the minimum in the instability ratio after which the stability is regained (dashed line in figure 8.5a). The growth rates indicate diffusion limitation before the 55 minute mark following a $1/\sqrt{t}$ dependence (dashed line in figure 8.5b), but continue to drop faster due to the depletion.

Kinetic data were taken by the described method from series of images of crystals growing under various conditions for a lysozyme concentration of 42 mg/ml (figures 8.7 and 8.8). Figure 8.7 shows corner-to-corner size and stabil-

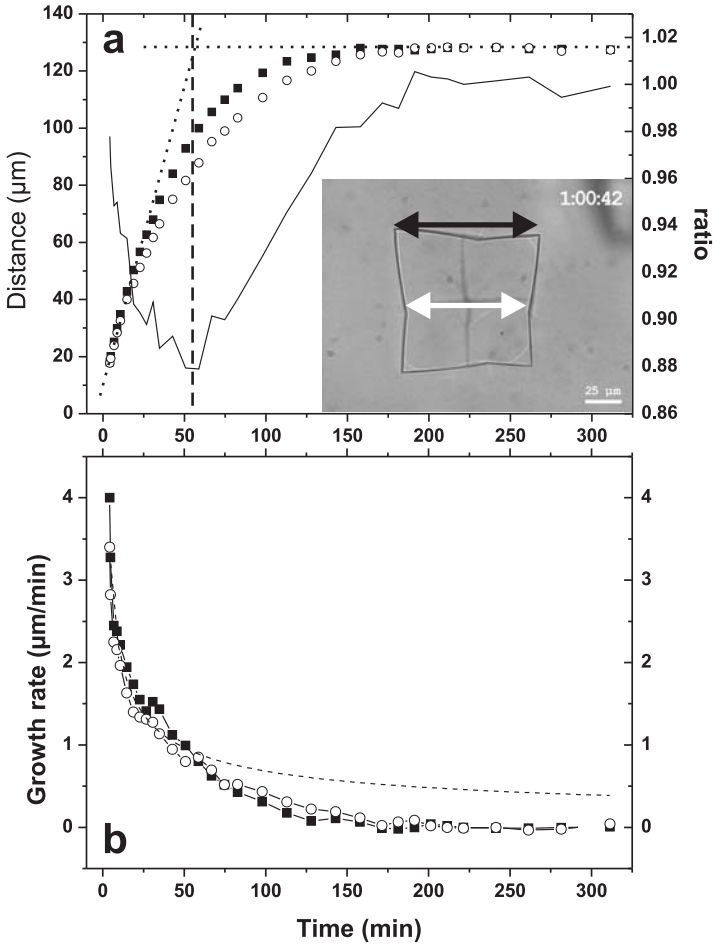


**Figure 8.5:** Growth data taken from the series of images in figure 8.1. (a) Squares indicate the distance between the top left and top right corner as indicated by the black arrow in the inset. Circles indicate the distance from the middle of the left (110) face to the right (110) face (white arrow in inset). The solid line depicts the ratio between corner-to-corner and middle-to-middle distance indicating instability when decreasing and smaller than 1. The dotted lines are slopes of the growth curve, the intersection of which indicates the moment at which the growth rate drops due to overlapping diffusion fields. (b) Growth rates of the corners (squares) and middle (circles) of the {110} faces. The dashed line indicates a $1/\sqrt{t}$ fit.

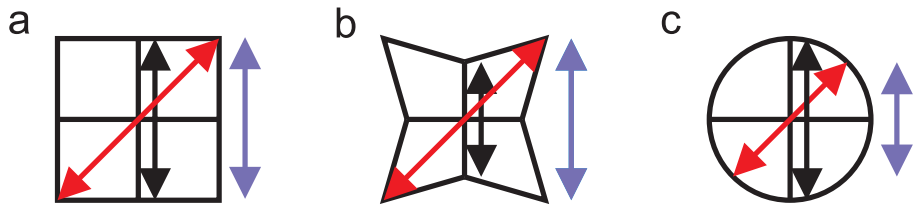


**Figure 8.6:** Schematic representation of the automatic acquisition of the dimensions of a crystal. The maximum (red arrows) and minimum diameter (black arrows) are acquired from the images. Via Pythagoras' theorem, the "corner-to-corner" distance is determined (blue arrows). The stability ratio is equal to the ratio between red, $L_{\text{centre}}$, and blue, $L_{\text{corner}}$, arrows. (a) The instability ratio is equal to 1 for stable crystals. (b) The instability ratio is smaller than 1 for morphologically unstable crystals. (c) For kinetically rough crystals the ratio is larger than 1.

ity ratio for experiments at 5 %w/v PEG and 10 %w/v PEG for temperatures ranging from 9 $^o$C to 21 $^o$C. Because the diffusion coefficient is only slightly temperature dependent, these data can be considered as function of $\Delta\mu/kT$. For 5 %w/v PEG the diffusion coefficient is approximately $3.7\times10^{-7}$ cm$^2$/s, while for 10 %w/v PEG the diffusion coefficient is approximately $2.1\times10^{-7}$ cm$^2$/s. For unstable crystals at 10 %w/v PEG, it takes longer to regain their stability than at 5%w/v PEG. Also, the ratio shows a slightly higher instability. At both PEG concentrations, crystals in the lower supersaturation experiment (i.e. higher temperatures) continue to grow for a longer time and to a larger size than crystals at high supersaturation. At high supersaturation, not only the growth rate but also the 3D-nucleation rate is high compared to low supersaturation. A higher number of crystals in the system speeds up the process of depletion of the mother liquor and thus the moment at which diffusion fields start to overlap.

Figure 8.8 shows size and stability ratio for experiments at 9 $^o$C and 15 $^o$C for PEG concentrations ranging from 0 %w/v to 10 %w/v. At higher PEG concentrations the crystals are polygonized and behave in the same way as those shown in figure 8.7. As the diffusion coefficient is lowered and $\Delta\mu/kT$

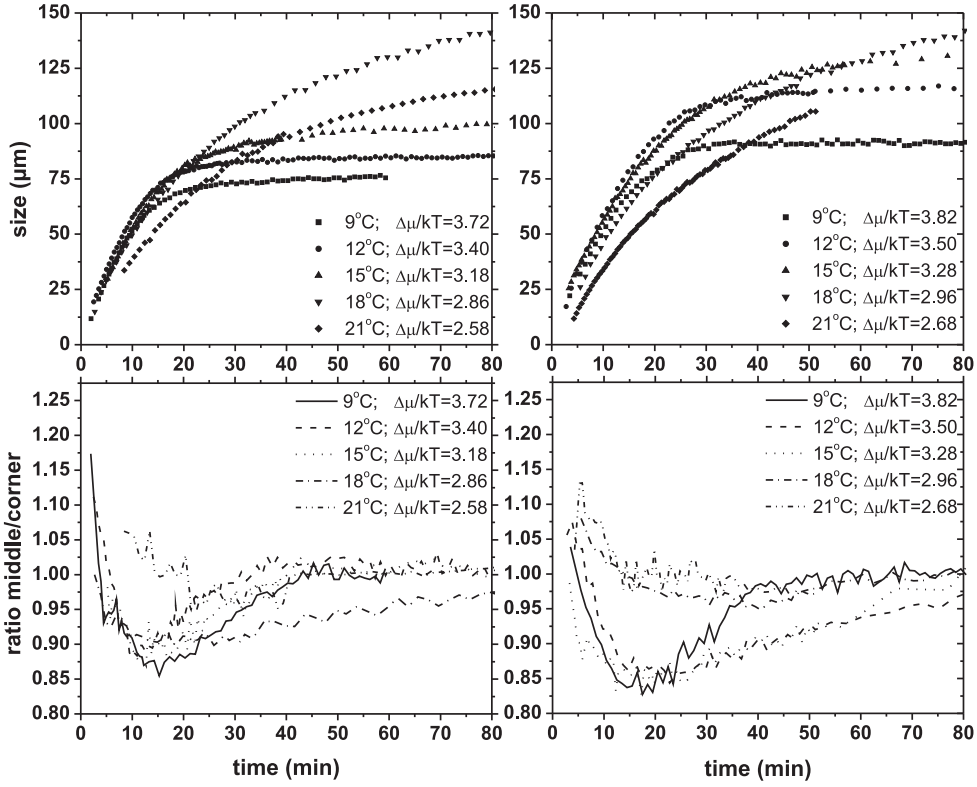


**Figure 8.7:** Kinetic data for 42 mg/ml HEWL, 0.685 M NaCl, 0.05M NaOAc/HOAc, pH 4.5, 5%w/v PEG-4600 (left column) and 10 %w/v PEG-4600 (right column) at various temperatures. The top row shows the corner-to-corner distance. The bottom row shows the instability ratio (see text).

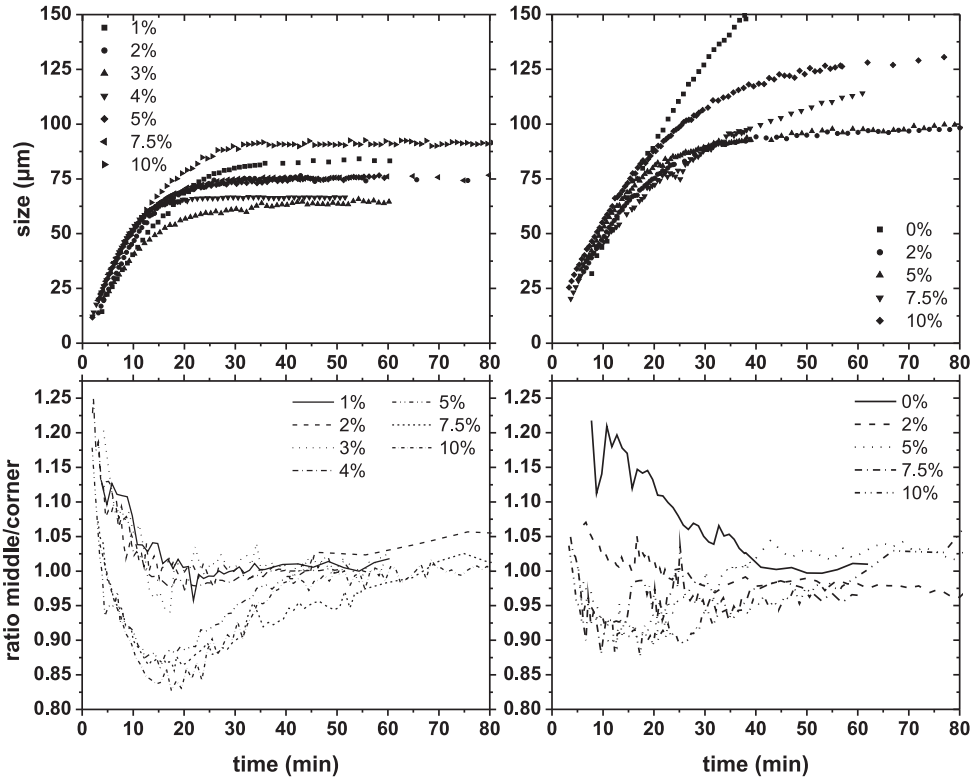


**Figure 8.8:** Kinetic data for 42 mg/ml HEWL, 0.685 M NaCl, 0.05M NaOAc/HOAc, pH 4.5 and various PEG concentrations at 9$^o$C (left column) and at 15$^o$C (right column). The top row shows the corner-to-corner distance. The bottom row shows the instability ratio (see text).

is increased, we expect a higher degree of morphological instability at these conditions. Experimental data show a general trend following this concept, but in detail are not consistent as a consequence of the 3D-nucleation effect as described above. Crystals grown at 15 $^o$C continue to grow to larger sizes than crystals grown at 9 $^o$C, confirming the influence of nucleation on growth kinetics (fig. 8.8). However, at lower PEG concentrations the situation is different. Here the crystals were found to be kinetically rough, resulting in a stability ratio larger than one. Thus, in general, crystals starting out rough stay stable throughout the experiment (figure 8.8, 9 $^o$C, 1-4%w/v PEG, and 15 $^o$C, 0 and 2%w/v PEG). In some experiments, at the rough-unstable transition line, the crystals start out slightly rough, develop facets as the supersaturation drops and enter in the polyhedral instability region and loose their stability (figure 8.9). In the end the solution is depleted and the crystal changes back to its faceted shape, thus having progressed through all morphological stages. The morphological changes are reflected in the stability ratio which starts at 1.18, drops to 0.88 and ends up at 1.0 (figure 8.8: 9$^o$C and 5% PEG).

In general, the shape of crystal, i.e. being faceted or being rounded due to roughening, appears to have a larger influence on the morphological stability than variations in $\Delta\mu$ and $D$.

### 8.3.4 2D nucleation versus step flow

To investigate qualitatively the influence of the finite dimensions of the crystal and its environment on the kinetics of a growing lysozyme crystal and its stability, we use a model based on the 2D nucleation rate and step velocity. At high supersaturations the formation of new layers occurs via "Birth and Spread", i.e. 2D nucleation and subsequent spread of the 2D islands over the crystal surface. Because the surface concentration for a polyhedral crystal is higher at its corners than in the middle, 2D nuclei are mainly formed at the corners. From here the layers spread out towards the middle of the crystal face (figure 8.2c). For a crystal to maintain its polyhedral shape, the average time for a new layer to nucleate should be at most equal to the time it costs for such a layer to cover the crystal surface. If nucleation of a new layer is

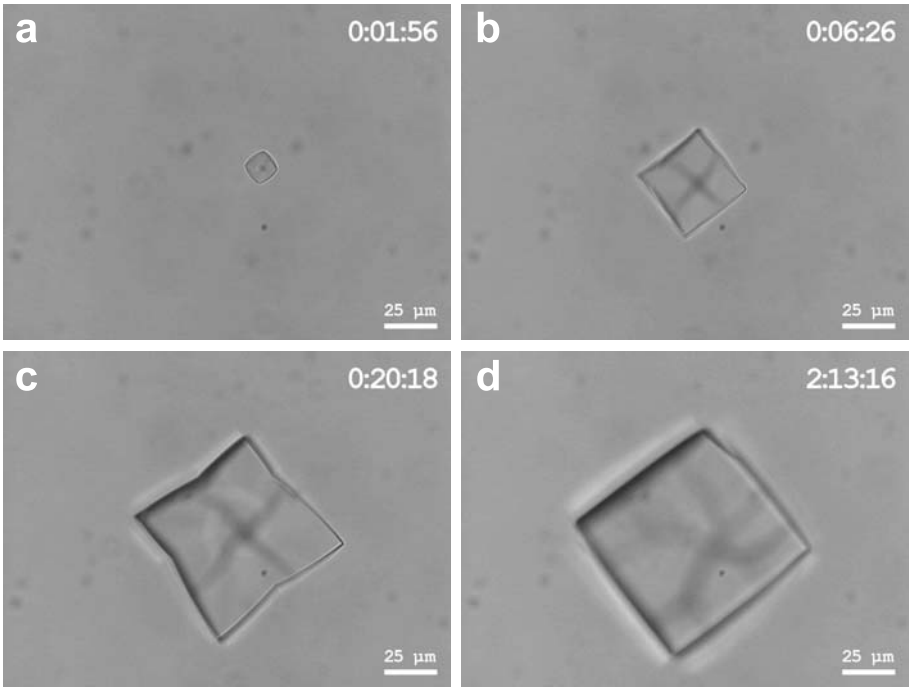


**Figure 8.9:** Tetragonal lysozyme crystal growing from a 42 mg/ml HEWL, 0.685 M NaCl, 0.05 M NaOAc/HOAc solution of pH 4.5 with 5 % PEG at 9 $^o$C. The crystal starts out kinetically rough (panel a), changes to faceted growth (panel b), subsequently looses its morphological stability (c), and in the end regains its stable, faceted shape (d). The scalebars indicate 25 $\mu$m.

faster, the corners will grow faster than the middle.

Thus, the shape of the crystal is determined by the balance between 2D nucleation at the edges and corners of the crystal and step flow at the face centre. Using this concept, we can perform the following analysis to find a relation between the local supersaturation and the local slope of the crystal surface. The step flux is constant over the surface and is equal to the nucleation rate, i.e. $J_{\mathrm{st}} = J_{\mathrm{nucl}}$. The step flux $J_{\mathrm{st}}$ is the number of steps passing the crystal surface at each point $x$ per unit time, and is the product of step velocity $v_{\mathrm{st}}(x)$ and the step density $\phi_{\mathrm{st}}(x)$, which is the number of steps per unit length:

$$J_{\mathrm{st}} = v_{\mathrm{st}}(x) \cdot \phi_{\mathrm{st}}(x) \ . \tag{8.7}$$

The step speed is given by

$$v_{\mathrm{st}}(x) = \beta_{\mathrm{st}} \cdot \sigma(x) \ , \tag{8.8}$$

in which $\beta_{\mathrm{st}}$ is the step kinetic coefficient, which we presume to be independent of step spacing. These two equations can be used to find an expression for the step density depending on nucleation rate and supersaturation:

$$\phi_{\mathrm{st}}(x) = \frac{J_{\mathrm{nucl}}}{\beta_{\mathrm{st}}\, \sigma(x)} \ . \tag{8.9}$$

Since the local slope of the surface, $p(x)$, is determined by the step density and the step height $h_{\mathrm{st}}$, i.e. $p(x) = \phi_{\mathrm{st}}(x) \cdot h_{\mathrm{st}}$, we now obtain an expression for the local slope

$$p(x) = \frac{J_{\mathrm{nucl}}\, h_{\mathrm{st}}}{\beta_{\mathrm{st}}\, \sigma(x)} \ . \tag{8.10}$$

The nucleation rate can be found by using the growth rate of the crystal at the corner, as the number of new layers is equal to the growth rate normal to the surface divided by the height of one layer, $J_{\mathrm{nucl}} = R_{\mathrm{corner}}/h_{\mathrm{st}}$. Thus, we find an expression for the local supersaturation as function of the local slope and the growth rate at the corner:

$$\sigma(x) = \frac{R_{\mathrm{corner}}}{\beta_{\mathrm{st}}} \cdot \frac{1}{p(x)} \ . \tag{8.11}$$

This expression can be used in analysing surface profiles taken from experiment. Figure 8.10a shows a time-lapse series of surface profiles of a morphologically unstable lysozyme crystal, and figure 8.10b shows the corresponding supersaturation profiles $\sigma(x) \cdot \beta_{\mathrm{st}}$, which is identical to $R_{\mathrm{corner}}/p(x)$. Determination of the actual supersaturation value $\sigma(x)$ is not possible as the step kinetic coefficient is not known. However, the supersaturation profiles are consistent within the experiment. Using equation 8.11, we find that the average supersaturation drops more than a factor of 10 during this growth run, whereas the supersaturation ratio between corner and middle of the crystal face remains roughly a factor two. The dotted line shows a typical surface profile for a square crystal growing by 2D nucleation as calculated using the finite differences method. When the stability is regained, the experimental supersaturation profiles have a shape similar to this calculated profile, which is typical for stable growth.

In section 8.3.3 we defined an instability criterion based on the ratio between the surface centre-to-centre distance $L_{\mathrm{centre}}$ and the corner-to-corner distance $L_{\mathrm{corner}}$. If growth is unstable this ratio decreases, and vice versa. An expression for this ratio can be given by

$$\frac{L_{\mathrm{centre}}}{L_{\mathrm{corner}}} = \frac{L_{\mathrm{corner}} - 2\lambda h_{\mathrm{st}}}{L_{\mathrm{corner}}} = 1 - \frac{2\lambda h_{\mathrm{st}}}{L_{\mathrm{corner}}} \ , \tag{8.12}$$

in which $\lambda$ is the number of steps the centre lags behind the corner, and $h_{\mathrm{st}}$ the height of one step. Although the slope $p(x)$ is not constant along the crystal surface, an average slope can be defined based on the corner-to-corner distance and the lag at the centre of the crystal surface:

$$\bar{p}(x) = \frac{\lambda h_{\mathrm{st}}}{\frac{1}{2} L_{\mathrm{corner}}} \ . \tag{8.13}$$

Substitution into equation 8.12 gives $L_{\mathrm{centre}}/L_{\mathrm{corner}} = 1 - \bar{p}(x)$. The change in $L_{\mathrm{centre}}/L_{\mathrm{corner}}$ with time, i.e. $\mathrm{d}(L_{\mathrm{centre}}/L_{\mathrm{corner}})/\mathrm{d}t$, is given by $-\mathrm{d}\bar{p}(x)/\mathrm{d}t$.

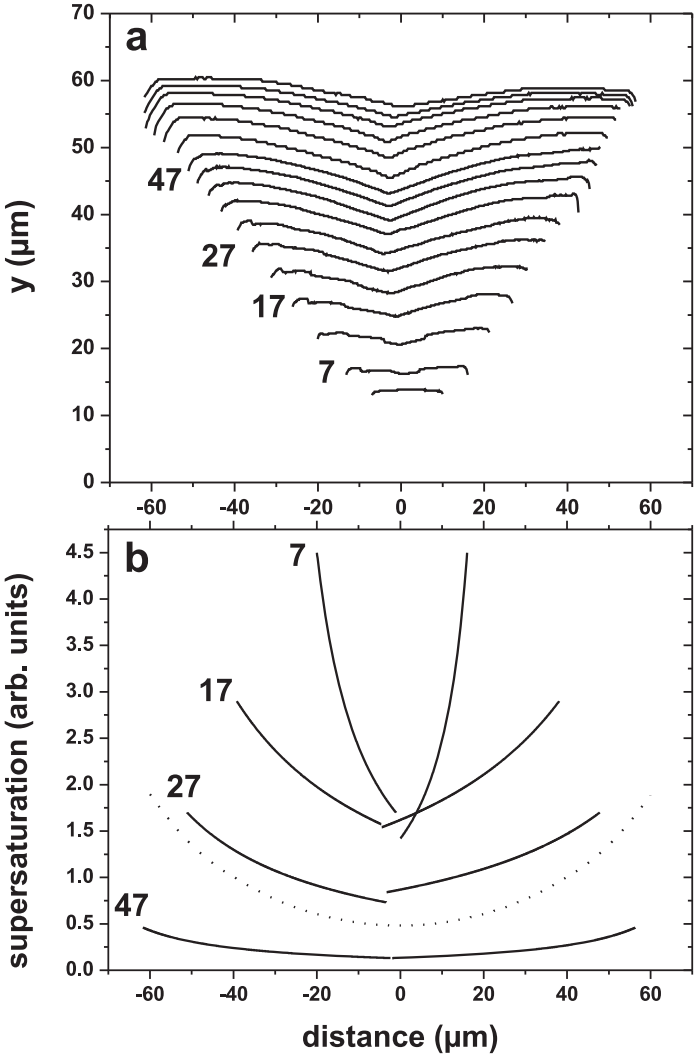


**Figure 8.10:** (a) Surface profiles extracted from time-lapse series of microscope images of a growing lysozyme crystal at 5 %w/v PEG-4600 and 18 $^o$C. Interval between succesive lines is approximately 5 minutes. (b) Relative supersaturation $\sigma$, proportional to $R_{\text{corner}}/p(x)$, derived from the surface profiles of panel (a) and the growth rate at the corner of the crystal. The dotted line indicates a typical surface profile of a square crystal growing by 2D nucleation, calculated by finite elements. The numbers indicate time in minutes.

In combination with equation 8.10 this results in

$$\begin{aligned} \frac{\mathrm{d}\left(\frac{L_{\mathrm{centre}}}{L_{\mathrm{corner}}}\right)}{\mathrm{d}t} &= -\frac{h_{\mathrm{st}}}{\beta_{\mathrm{st}}}\frac{\mathrm{d}\left(J_{\mathrm{nucl}} < \frac{1}{\sigma(x)} >\right)}{\mathrm{d}t} \\ &= -\frac{h_{\mathrm{st}}}{\beta_{\mathrm{st}}}\frac{\mathrm{d}\left(J_{\mathrm{nucl}}/\sigma_{\mathrm{avg}}\right)}{\mathrm{d}t} \ , \end{aligned} \tag{8.14}$$

with $\sigma_{\mathrm{avg}}$ is $< 1/\sigma(x) >^{-1}$. For 2D nucleation the supersaturation dependent nucleation rate is approximated by[39]

$$\begin{aligned} J_{\mathrm{nucl}} &\cong A'(v_{\mathrm{step}})_{\mathrm{corner}} \exp\left\{-\frac{B}{\Delta\mu_{\mathrm{corner}}/kT}\right\} \\ &= A'\beta_{\mathrm{st}}\sigma_{\mathrm{corner}} \exp\left\{-\frac{B}{\ln(\sigma_{\mathrm{corner}}+1)}\right\} \ , \end{aligned} \tag{8.15}$$

with $A'$ and $B$ supersaturation independent coefficients, and $\sigma_{\mathrm{corner}}$ the supersaturation at the corners of the crystal. Thus, by combining equation 8.14 and 8.15 the change in (in)stability ratio becomes

$$\frac{\mathrm{d}\left(\frac{L_{\mathrm{centre}}}{L_{\mathrm{corner}}}\right)}{\mathrm{d}t} = -\frac{\mathrm{d}\left(A\frac{\sigma_{\mathrm{corner}}}{\sigma_{\mathrm{avg}}}\exp\left\{-\frac{B}{\ln[\sigma_{\mathrm{avg}}+1]}\right\}\right)}{\mathrm{d}t} \ . \tag{8.16}$$

Evaluating equation 8.16 in combination with figure 8.10 we find three regions of interest. For small crystals, i.e. at the start of the experiment, the surface profile is a straight line without a cusp (bottom profile in fig. 8.10a), indicating that $\sigma_{\mathrm{corner}} \approx \sigma_{\mathrm{avg}}$. 2D nucleation occurs on the whole crystal surface, which is planar. Next, the crystals become larger and as a result the ratio $\sigma_{\mathrm{corner}}/\sigma_{\mathrm{avg}}$ increases, while the change in the exponential term does not play a role yet. The ratio $L_{\mathrm{centre}}/L_{\mathrm{corner}}$ decreases, which indicates loss of stability. During continued growth of the crystals, the overall concentration in the finite system goes down and as a result also the surface concentration decreases. Now the exponential term in equation 8.16 plays a major role as its value drops rapidly and $\mathrm{d}(L_{\mathrm{centre}}/L_{\mathrm{corner}})/\mathrm{d}t$ becomes positive, which makes the ratio $L_{\mathrm{centre}}/L_{\mathrm{corner}}$ going back to 1. Thus, stability is regained even though the ratio $\sigma_{\mathrm{corner}}/\sigma_{\mathrm{avg}}$ remains larger than 1. In the end the system is depleted from growth units and the surface concentration drops to the region of spiral growth, in which the crystal finds its stable form[20].

## 8.4 Conclusions

Polyhedral instability for lysozyme crystals was previously estimated to occur for crystals larger than 2 cm. We have shown that by the addition of PEG-4600 the balance between surface kinetics and mass transport can be shifted such that instability occurs for crystals a mere 30 $\mu$m in size. In-situ measurements using optical microscopy showed that the morphological stability of the crystals decreases for higher driving force and lower solute diffusion coefficients. However, if the crystal is kinetically roughened the situation differs and stability increases for increasing driving force, which can be explained by the rounded shape deviating from the polyhedral shape of the crystal. Due to the finite supply of lysozyme in the system crystals regain their stability, not revealing their history of instability. Thus, a look at crystals at the end of an experiment does not necessarily reveal any processes detrimental to crystal quality. Changing crystallization conditions during growth based upon in-situ observations may avoid the occurrence of morphological instability while retaining the high initial supersaturation needed for nucleation. A qualitative model based on the balance between 2D nucleation at the corners of the crystal and step velocity toward the middle explains the influence of mass transport on stability and shows the regain of stability when the supply of growth units runs dry.

## References

[1] Luft, J.; Collins, R.; Fehrman, N.; Lauricella, A.; Veatch, C.; DeTitta, G. *J. Struc. Biol.* **2003,** *142,* 170-179.

[2] Hennessy, D.; Buchanan, B.; Subramanian, D.; Wilkosz, P.; Rosenberg, J. *Acta Crystallogr., Sect. D: Biol. Crystallogr.* **2000,** *56,* 817-827.

[3] Zheng, B.; Roach, L.; Ismagilov, R. *J. Am. Chem. Soc.* **2003,** *125,* 11170-11171.

[4] Cudney, R.; Patel, S.; Weisgraber, K.; Newhouse, Y.; McPherson, A. *Acta Crystallogr., Sect. D: Biol. Crystallogr.* **1994,** *50,* 414-423.

[5] Bhat, R.; Timasheff, S. *Protein Sci.* **1992,** *1,* 1133-1143.

[6] Atha, D.; Ingham, K. *J. Biol. Chem.* **1981,** *256,* 2108-2117.

[7] Vivarès, D.; Bonneté, F. *Acta Crystallogr., Sect. D: Biol. Crystallogr. 58,* 472-479.

[8] Vergara, A.; Capuano, F.; Paduano, L.; Sartorio, R. *Macromolecules* **2006,** *39,* 4500-4506.

[9] Kundrot, C.; Judge, R.; Pusey, M.; Snell, E. *Cryst. Growth Des.* **2001,** *1,* 87-99.

[10] Carter, D.; Rhodes, P.; McRee, D.; Tari, L.; Dougan, D.; Snell, G.; Abolac, E.; Stevens, R. *J. Appl. Crystallogr.* **2005,** *38,* 87-90.

[11] Cherezov, V.; Caffrey, M. *J. Appl. Crystallogr.* **2003,** *36,* 1372-1377.

[12] Robert, M.; Lefaucheux, F. *J. Cryst. Growth* **1988,** *90,* 358-367.

[13] Biertümpfel, C.; Basquin, J.; Suck, D.; Sauter, C. *Acta Crystallogr., Sect. D: Biol. Crystallogr.* **2002,** *58,* 1657-1659.

[14] Garcia-Ruiz, J.; Moreno, A.; Viedma, C.; Coll, M. *Mater. Res. Bull.* **1993,** *28,* 541-546.

[15] Poodt, P.; Heijna, M.; Tsukamoto, K.; de Grip, W.; Christianen, P.; Maan, J.; van Enckevort, W.; Vlieg, E. *Appl. Phys. Lett.* **2005,** *87,* Art. No. 214105.

[16] Snell, E.; Helliwel, J. *Rep. Progr. Phys.* **2005,** *68,* 799-853.

[17] Lin, H.; Rosenberger, F.; Alexander, J.; Nadarajah, A. *J. Cryst. Growth* **1995,** *151,* 153-162.

[18] Chernov, A. *J. Cryst. Growth* **1974,** *24-25,* 11-31.

[19] Wilcox, W. *J. Cryst. Growth* **1977,** *38,* 73-81.

[20] Kuroda, T.; Irisawa, T.; Ookawa, A. *J. Cryst. Growth* **1977,** *42,* 41-46.

[21] Vekilov, P.; Rosenberger, F. *J. Cryst. Growth* **1996,** *158,* 540-551.

[22] Heijna, M.; van den Dungen, P.; van Enckevort, W.; Vlieg, E. *Cryst. Growth Des.* **2006,** *6,* 1206-1213.

[23] Nanev, C.; Penkova, A. *J. Cryst. Growth* **2002,** *237-239,* 283-288.

[24] Wilcox, W. *J. Cryst. Growth* **1983,** *65,* 133-142.

[25] McEwan, A.; Ristic, R.; Shekunov, B.; Sherwood, J. *J. Cryst. Growth* **1996,** *167,* 701-708.

[26] Vekilov, P.; Alexander, J.; Rosenberger, F. *Phys. Rev. E* **1996,** *54,* 6650-6660.

[27] ImagePro Plus 4.5, MediaCybernetics.

[28] MATLAB 6.5 (Release 13), The MathWorks Inc.

[29] Berg, W. *Proc. R. Soc. London, A* **1938,** *164,* 79-95.

[30] Seeger, A. *Philos. Mag.* **1953,** *44,* 1-13.

[31] Mullins, W.; Sekerka, R. *J. Appl. Phys.* **1963,** *34,* 323.

[32] Mullins, W.; Sekerka, R. *J. Appl. Phys.* **1964,** *35,* 444.

[33] Gorti, S.; Forsythe, E.; Pusey, M. *Cryst. Growth Des.* **2004,** *4,* 691-699.

[34] van Veenendaal, E.; van Hoof, P.; van Suchtelen, J.; van Enckevort, W.; Bennema, P. *Surf. Sci.* **1998,** *417,* 121-138.

[35] Forsythe, E.; Judge, R.; Pusey, M. *J. Chem. Eng. Data* **1999,** *44,* 637-640.

[36] Muschol, M.; Rosenberger, F. *J. Chem. Phys.* **1995,** *103,* 10424-10432.

[37] Tanford, C. *Physical Chemistry of Macromolecules;* Wiley: New York, 1961.

[38] Heijna, M.; Theelen, M.; van Enckevort, W.; Vlieg, E. *J. Phys. Chem. B* **2007,** *111,* 1567-1573.

[39] van der Eerden, J. . In *Handbook of Crystal Growth*; Elsevier Science Publishers: Amsterdam, 1993.